Journal of
Mechanics of
Materials and Structures

EFFECTS OF SURFACE DEFORMATION ON THE COLLECTIVE BUCKLING
OF AN ARRAY OF RIGID BEAMS ON AN ELASTIC SUBSTRATE

Haojing Lin, Ziguang Chen, Jiashi Yang and Li Tan

EFFECTS OF SURFACE DEFORMATION ON THE COLLECTIVE BUCKLING OF AN ARRAY OF RIGID BEAMS ON AN ELASTIC SUBSTRATE

HAOJING LIN, ZIGUANG CHEN, JIASHI YANG AND LI TAN

We analyze the collective buckling of a row of rigid beams with their lower ends built into an elastic substrate. The beams interact among themselves through the deformation of the substrate. The present analysis is more sophisticated than previous ones in that the lower ends of the beams are allowed to move vertically and horizontally, in addition to rotation. From the linear theory of elasticity and rigid body statics, an eigenvalue problem is formulated and solved. Calculations showed that periodic deformations resulted atop the compliant substrate after restrictions on the beam base displacements were released. Consequently, the refined model found good match with the height measurements from Atomic Force Microscope (AFM). Our work suggests that both the compliant substrate and the interaction of neighboring beams through the deformation of the substrate dominate the collective buckling. Furthermore, these results contribute toward the understanding, design and application of soft nanostructures produced by soft lithography in a variety of fields.

1. Introduction

Periodic arrays of 100 nm thick and wide beams and walls composed of elastic polymers can be manufactured on a surface of the same material by soft lithography [Xia and Whitesides 1998], nanoimprint lithography [Chou et al. 1995; 1996] and other techniques. Thermal, electrical or magnetic features can also be added to the structures [Liu et al. 2010] such that they are useful in a variety of fields like optical gratings, sensor arrays, actuators, and nanofabrication. Due to the deformability of the soft structures and the substrates, structural instability is a common issue in soft lithography. This results in buckling or collapsing of the structures [Xia and Whitesides 1998; Chou et al. 1995; 1996; Delamarche et al. 1997; Schmid and Michel 2000; Evans et al. 2007], which seriously affects their functionality and limits their applications.

The buckling of soft nanostructures has aspects that are different from conventional structural engineering and it has recently caught wider attention. What is unique is that the substrate of the structures is very compliant so that neighboring structures interact through the deformation of the substrate. The results from the buckling analysis in conventional structural engineering are usually for a single beam [Greenhill 1881; Timoshenko 1936]. Some of the structural engineering results are relevant for the buckling of soft nanostructures, e.g., the buckling of a beam under its own weight [Greenhill 1881]; the buckling of a beam resting on an elastic foundation [Timoshenko 1936]; and the lateral torsional buckling of a high aspect ratio beam [Alfutov 2000]. The results from structural engineering on the buckling of elastic beams were used in [Hui et al. 2002] for the buckling of a single beam and the contact of two beams on a buckled surface in soft lithography, but the substrate deformation and the beam interaction

through the substrate were not considered. Therefore the results in [Hui et al. 2002] can only provide limited understanding of the situation.

A major progress in the buckling analysis of periodic soft nanostructures was made in our recent work [Lin et al. 2007]. Due to the inclusion of the most basic and important mechanism into our theoretical model, i.e., neighboring beams interact through the deformation of the substrate, we were able to describe the most basic collective buckling behavior of the soft structures and obtain results qualitatively matching experimental findings. The model in [Lin et al. 2007] was later generalized and applied to the case of a two-dimensional array of rigid beams on an elastic foundation [Chen et al. 2008], a nonuniform one-dimensional array of rigid beams [Li et al. 2010], and a one-dimensional array of elastic beams [Feng and Li 2009; Lin et al. 2010].

In [Lin et al. 2007; Chen et al. 2008; Li et al. 2010; Feng and Li 2009; Lin et al. 2010], the beam bottoms in the substrate were allowed to rotate which is the major deformation, but their vertical and horizontal displacements were neglected. While this could describe the collective buckling of beam arrays, the restriction on beam bottom displacements renders the system too stiff. Therefore there remains an issue on the effect of horizontal and vertical displacements of the beam bottoms.

In this paper we generalize the analysis in [Lin et al. 2007] by removing the restrictions on the beam bottom displacements. The bottoms of the beams can move in both horizontal and vertical directions. The results show periodic deformations atop the compliant substrate and such behaviors closely match with the experimental evidence.

2. Mechanics model

Consider the structure shown in Figure 1, which consists of an array of rigid beams on an elastic substrate. Each beam represents the cross section of a wall that extends uniformly in the direction perpendicular to the plane of the paper. There is no displacement and no variation in this direction. A unit thickness of the structure in the direction perpendicular to the paper is taken. We have a so-called plane-strain problem in elasticity. Weight has often been considered as the cause of buckling [Hui et al. 2002; Sharp et al. 2004]. Other effects including van der Waals, Coulomb, or capillary forces could also contribute to the situation [Evans et al. 2007; Chuang et al. 2005; Hsia et al. 2005]. We will consider weight below as the
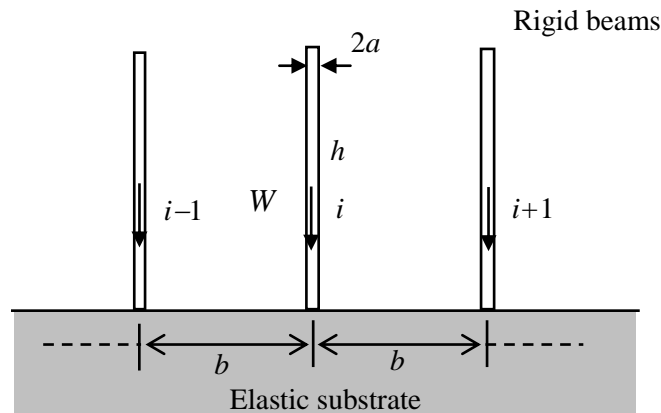

Figure 1. A system of rigid beams on an elastic substrate.
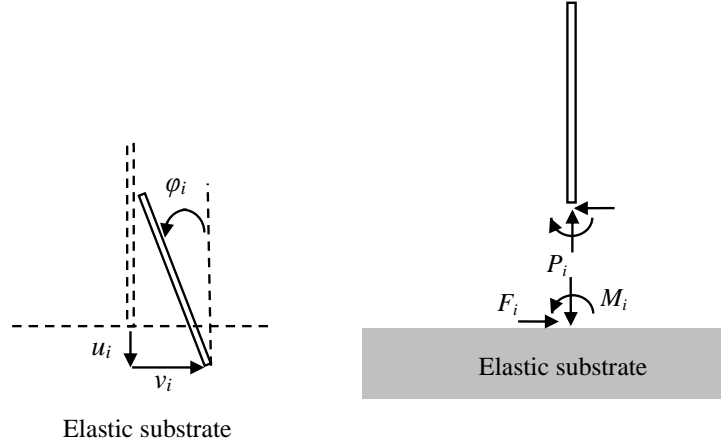
Figure 2. End displacements and end forces of a typical beam.

only load and the substrate deformability as the only interaction. Effectively other possible forces either modify the load or the interaction coefficients in our model. The weight of the beams is considered as the resultant of a uniformly distributed load. The intensity of the load is given by q per unit length of the beams. Let the height and width of the beams be h and $2a$, and the spacing between the center lines of two neighboring beams be b (see Figure 1). We have $q = \rho g 2a$. The weight $W = \rho g 2ah$ acts at the center of the beam. The beams are assumed to be rigid, as in [Lin et al. 2007; Chen et al. 2008; Li et al. 2010]. In contrast with these works (and also with [Feng and Li 2009] and [Lin et al. 2010]), here we allow the bottoms of the beams to move in both the horizontal and vertical directions, in addition to rotation. The substrate is modeled as an elastic half-space.

For the bottom of a typical beam, with index i, let the vertical and horizontal displacements be u_i and v_i, the vertical and horizontal forces P_i and F_i, the rotation φ_i, and the moment M_i (see Figure 2).

For simplicity we construct the two vectors

$$\boldsymbol{u}_i = \begin{Bmatrix} u_i \\ v_i \\ \varphi_i \end{Bmatrix}, \qquad \boldsymbol{f}_i = \begin{Bmatrix} P_i \\ F_i \\ M_i \end{Bmatrix}, \tag{1}$$

whose components are shown in Figure 2. Within the linear theory of elasticity, by superposition, we can write

$$\boldsymbol{u}_i = \sum_{j=1}^{\infty} \boldsymbol{A}_{ij} \boldsymbol{f}_j \cong \boldsymbol{A}_{i(i-1)} \boldsymbol{f}_{i-1} + \boldsymbol{A}_{ii} \boldsymbol{f}_i + \boldsymbol{A}_{i(i+1)} \boldsymbol{f}_{i+1}, \tag{2}$$

where the A_{ij} are 3×3 matrices whose columns representing the substrate deformation at the i-th location due to a unit load at the j-th location only, the loads at all other locations being zero. The A_{ij} can be derived from the theory of elasticity; see the Appendix. Equation (2) can be inverted to yield

$$\boldsymbol{f}_i = \sum_{j=1}^{\infty} \boldsymbol{B}_{ij} \boldsymbol{u}_j \cong \boldsymbol{B}_{i(i-1)} \boldsymbol{u}_{i-1} + \boldsymbol{B}_{ii} \boldsymbol{u}_i + \boldsymbol{B}_{i(i+1)} \boldsymbol{u}_{i+1} \tag{3}$$

where the columns of B_{ij} represent the load at the i-th location due to a unit deformation at the j-th
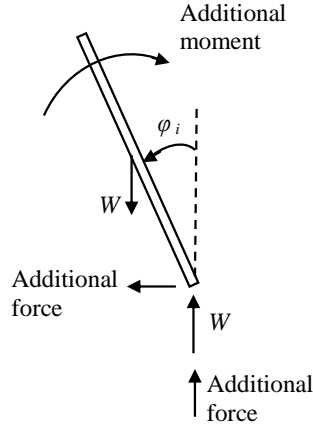
Figure 3. Free body diagram of a buckled beam.

location only, the deformations at all other locations being zero. In (3) and (4) we have made an approx-
imation by considering interactions between a beam and its two immediate neighbors, which is known
to be accurate enough for what we are interested [Li et al. 2010]. Long distance interactions among
nonneighboring beams are neglected.

When the i-th beam buckles, its free body diagram is shown in Figure 3, where the vertical load W
and the corresponding vertical reaction with the same magnitude exist in both the unbuckled and buckled
states. The rest are possible additional loads due to buckling. The equilibrium of the beam requires that

$$
\sum_{j=1}^{\infty} \left([\boldsymbol{B}_{ij}]_{11} u_j + [\boldsymbol{B}_{ij}]_{12} v_j + [\boldsymbol{B}_{ij}]_{13} \varphi_j \right) = 0,
$$

$$
\sum_{j=1}^{\infty} \left([\boldsymbol{B}_{ij}]_{21} u_j + [\boldsymbol{B}_{ij}]_{22} v_j + [\boldsymbol{B}_{ij}]_{23} \varphi_j \right) = 0, \tag{4}
$$

$$
-W \frac{h}{2} \varphi_i + \sum_{j=1}^{\infty} \left([\boldsymbol{B}_{ij}]_{31} u_j + [\boldsymbol{B}_{ij}]_{32} v_j + [\boldsymbol{B}_{ij}]_{33} \varphi_j \right) = 0.
$$

Equations $(4)_1$ and $(4)_2$ say that the additional horizontal and vertical forces due to buckling are zero,
while $(4)_3$ is the moment equation about the bottom of the beam. In (4), $[B_{ij}]_{11}$ represents the $(1,1)$
element of the 3×3 matrix B_{ij}, and the rest are similar. In (4) we have a system of linear homogeneous
equations. The trivial solution with all $\boldsymbol{u}_i = 0$ is the unbuckled state. We are interested in nontrivial
solutions of (4) representing buckled states. Then (4) is an eigenvalue problem. We look for values of
$Wh/2$ corresponding to which nontrivial solutions of $\boldsymbol{u}_i$ exist.

3. Numerical results and discussion

As an example, we still consider the same twenty beams as in [Lin et al. 2007] with the same geometric
and material parameters. The system (4) is solved numerically on a computer. Within three significant
digits, the numerical results for the eigenvalues $Wh/2$ are those in Table 1. They are the same as those
in [Lin et al. 2007], where the beam bottom horizontal and vertical displacements were not allowed.

8.96	9.00	9.05	9.13	9.23	9.34	9.48	9.63	9.80	9.98
10.16	10.36	10.55	10.74	10.92	11.08	11.23	11.35	11.43	11.49

Table 1. Numerically calculated eigenvalues $Wh/2$ for the 20-beam system, in nN.

The buckled states determined from the eigenvectors are different from the previous analysis and are shown in Figure 4, left, where they are also ranked according to the magnitude of the eigenvalues. Even though the buckled states near the bottom and top of the figure have a one-to-one correspondence with the results of [Lin et al. 2007], the ones near the middle of the figure differ from the corresponding ones in that reference by having both rotation rearrangements and surface deformations. The latter change is the new finding by relaxing restrictions on displacement of beam bases. We enlarged the calculated surface topographies in Figure 4, right, to view the details of such change. Among the twenty instability modes, all the substrates have a periodic, wave-like feature where topography fluctuates between landmarks like hilltops and valleys. The periodicity of the fluctuation gradually increases from 400 nm in mode #1 to more than 4000 nm in mode #20. In contrast, amplitude variance is more complex. Figure 5, left, indicates the contrast between two fluctuating surfaces with minimum and maximum amplitudes, where a 6-fold difference in the magnitude of the amplitude is observed between mode #13 and #1. Qualitatively, this proves that more energy is needed to cause instability such as in mode #13.

In Figure 5, right, we superposed beam locations atop the fluctuating surface topographies. It is clear that the multibeam-like buckling feature is mostly concentrated in valleys. In other words, the beams having a larger tendency to rotate will result in more significant displacements on bases, giving rise to noticeable up- or downhill portions in topography. More interestingly, since the buckled features
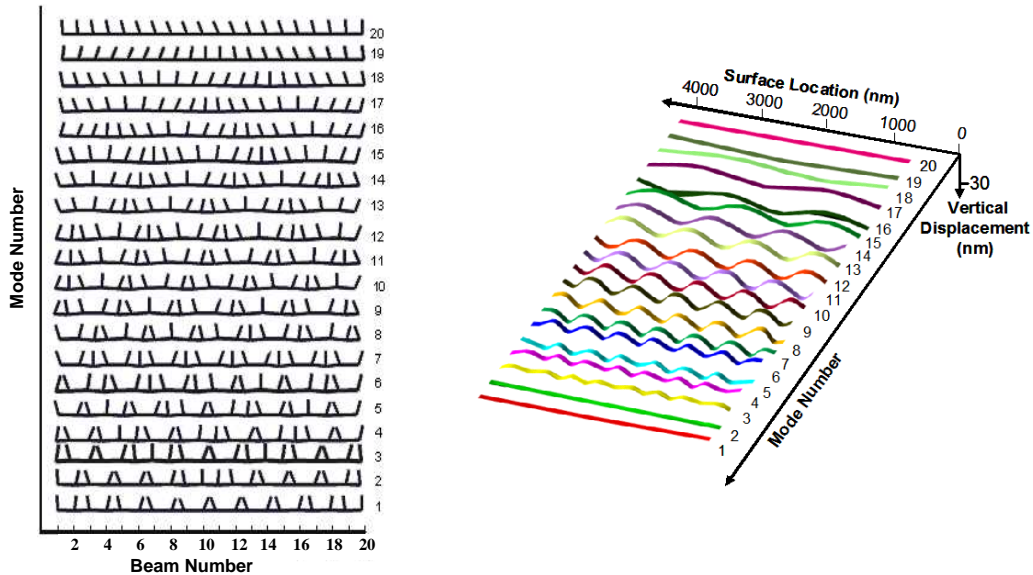

Figure 4. Theoretical results of collective buckling. Left: Buckled beams and substrate deformation. Right: surface fluctuations in each individual buckling mode. Both graphs show modes ranked by the magnitude of their eigenvalues.
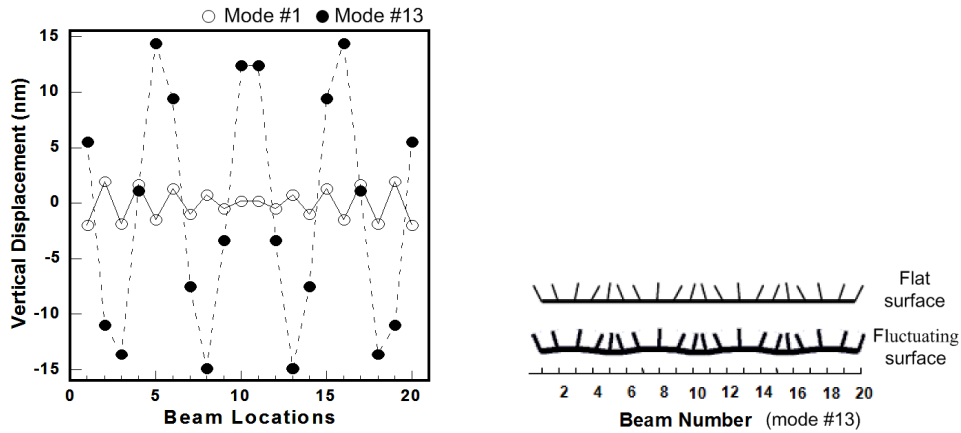
Figure 5. Theoretical results of collective buckling. Left: surface topographies of buckling modes with the maximum (#13) and minimum (#1) fluctuations. Right: comparison of beam displacements and rotations atop a flat surface (model in [Lin et al. 2007]) and a fluctuating surface (current model).

are all localized in the valleys of the fluctuated surfaces, open surfaces will reside on hilltops of those fluctuations. This latter statement could help us to understand the following experimental results more accurately than before.

To give us a visual picture of the buckling in soft nanostructures, we used the easy-to-perform process of embossing/imprinting lithography [Chou et al. 1996; Xia and Whitesides 1998] and created periodic nanostructures atop an elastic poly(dimethylsiloxane) (PDMS) substrate. The soft nanostructure was formed by spin-coating the PDMS precursor mixture on a rigid mold and baking at an elevated temperature for an extended period of time. To obtain a uniform pattern on PDMS, it is necessary to treat the rigid mold (Si or SiO_2 with grating lines with a pitch size of 200 nm, a linewidth of 100 nm and a depth of 150 nm) with O_2 plasma, followed by a perfluorosilane treatment in toluene (0.2 M, 5 min). The soft nature of the PDMS material, plus the high aspect ratio of the copied nanostructures from the mold, suggest an appearance of collective buckling, as we mentioned before.

We used atomic force microscopy (AFM) to evaluate the topography of the buckled lines. The advantages of AFM are that it is a high-resolution imaging tool, which allows us to survey the overall buckling of soft structures at the nanometer scale; and that the noncontact nature of the AFM tapping mode eliminates any contact forces between the tip and the underlying nanostructure.

Figure 6, left, shows the topography of the rigid stamp with one-dimensional grating features. The resulting PDMS copies show extensive surface buckling features, displayed in by Figure 6, middle, where both multibeam and multimode buckling phenomena are in evidence, and which we discuss in more detail shortly.

The first case of instability in Figure 4 (mode #1, two-beam pairing) has been observed by several researchers [Delamarche et al. 1997; Xia and Whitesides 1998; Hui et al. 2002; Chuang et al. 2005] during nanofabrication, and is often used as a classic picture for nanostructure buckling. In those findings, a rigid substrate backing or a thick PDMS sample are often selected to limit large deformation to the
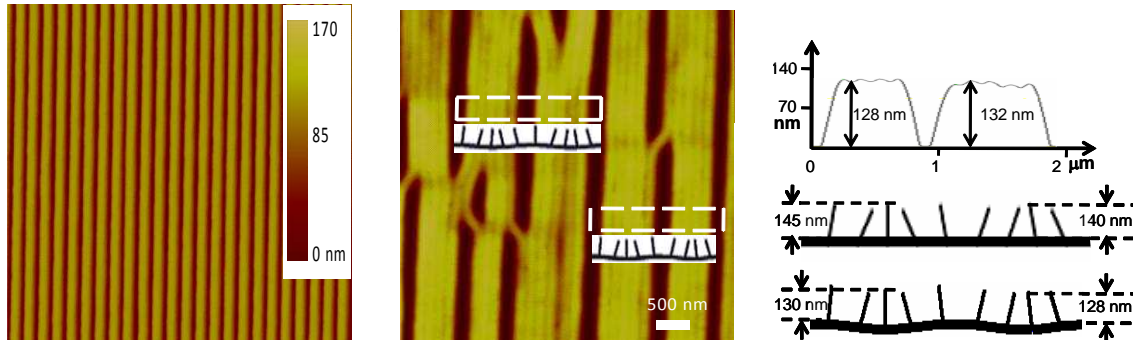
Figure 6. AFM topographical images and cursor plots of a rigid mold and fabricated PDMS structures from embossing/imprinting. Left: original mold with a pitch of 200 nm and a depth of 150 nm. Middle: multibeam and multimode buckling features, with superimposed sketches showing rotations of individual beams in selected areas: collective buckling follows mode #12 in the upper area and mode #13 in the lower area, as predicted by Figure 4. A branching angle of 45° is evident in boundaries between two different buckled patches. Right: cursor plot of bucked features in the middle figure, and comparison with theoretical calculations.

stamp material [Schmid and Michel 2000], so minimum energy impact is ensured for the occurrence of pairing. In contrast, when no precautions are taken with the stamp material or when substantial deformation occurs in the nanostructuring process, multibeam buckling modes at higher energy levels should be expected; the fluctuation of those energy impacts could even generate multiple buckling modes.

We saw a good match of these predictions in our experimental data, as exemplified in Figure 6. For example, selected areas of Figure 6, middle, match with predicted buckling modes #12 and #13; these modes are sketched underneath the corresponding areas in the figure. A branching angle of 45° between the two neighboring buckling modes suggests a shear or rotation nature of these impacts, validating our approximation of buckling in elastic beams with rotation of rigid ones.

In Figure 6, top right, we see the cursor plot of AFM measurements for one of the buckling features, indicating a depth value of 128–132 nm for those landmarks. We saw a mismatch between this number with our previous analysis in [Lin et al. 2007]. When the restriction on beam displacements is not released, as in that earlier reference, the feature depth in buckled beams is expected to depend mainly on the rotation of beams. When minimal rotation is assumed, the depth should be close to the depth of the rigid mold ($h = 150$ nm).

The middle portion of Figure 6, right, illustrates the buckled beams in such a condition, where beams are resting on a flat ground and the height difference, i.e., 140–145 nm, between the top center of the multibeam and the open area is calculated. Clearly, our experimental data suggest otherwise; and the number obtained is more than 13% smaller than what we have estimated. While difficult to explain from our previous modeling results in [Lin et al. 2007], this could be justified by taking beam displacements into consideration. Figure 6, bottom right, shows the buckled beams without the restriction on beam displacements. Surface fluctuation from the base lowered the height of the multibeam and simultaneously increased the level of hilltops in open areas. Accordingly, the new calculation leads to a value for the

beam depth of 128–130 nm, much closer to the observed one. Overall, this analysis supplies the refined model with good experimental evidence.

4. Conclusion

A mechanical model is developed for analyzing the collective buckling of an array of beams on an elastic substrate; it includes the refinement of allowing the bottom of the beams to move both horizontally and vertically, as well as rotating. Numerical results from the model show that periodic surface deformations resulted atop the compliant substrate, which found a better match with the height measurements from AFM. Our work suggests that both the compliant substrate and the interaction of neighboring structures through the deformation of the substrate dominate the collective buckling. This makes the buckling of periodic soft nanostructures unique and different from conventional structural engineering.

Acknowledgments

Appendix: Calculation of A_{ij}

First consider the case of a vertical load on a half-space in plane-strain elasticity (see Figure 7). The stress and displacement fields are given in [Timoshenko and Goodier 1970]:

$$\sigma_r = -\frac{2P}{\pi}\frac{\cos\theta}{r}, \quad \sigma_\theta = 0, \quad \tau_{r\theta} = 0,$$

$$u = -\frac{2P}{\pi E}\cos\theta \ln\frac{r}{d} - \frac{(1-v)P}{\pi E}\theta\sin\theta, \tag{5}$$

$$v = \frac{(1+v)P}{\pi E}\sin\theta - \frac{(1-v)P}{\pi E}\theta\cos\theta + \frac{2P}{\pi E}\sin\theta\ln\frac{r}{d}, \tag{6}$$

$$\frac{1}{2}\left(\frac{\partial v}{\partial r} - \frac{1}{r}\frac{\partial u}{\partial\theta} + \frac{v}{r}\right) = \frac{2P}{\pi E}\frac{\sin\theta}{r} \tag{7}$$
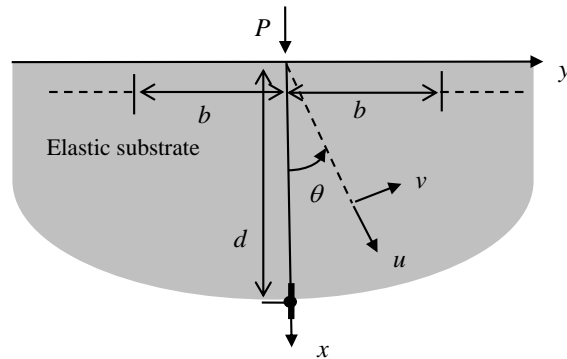

Figure 7. A half-space under a vertical load.

In obtaining (5)–(7), the following conditions are imposed at $\theta = 0$ and $r = d$ for determining the displacement field uniquely:

$$u = 0, \qquad v = 0, \qquad \frac{\partial v}{\partial r} = 0. \tag{8}$$

The value of d serves as a common reference point. From (5)–(7) we calculate

$$[A_{i(i-1)}]_{11} = -v(b, \pi/2) = -\frac{(1+v)P}{\pi E} - \frac{2P}{\pi E} \ln \frac{b}{d},$$

$$[A_{i(i-1)}]_{21} = u(b, \pi/2) = -\frac{(1-v)P}{2E},$$

$$[A_{i(i-1)}]_{31} = \frac{1}{2}\left(\frac{\partial v}{\partial r} - \frac{1}{r}\frac{\partial u}{\partial \theta} + \frac{v}{r}\right)_{r=b, \theta=\pi/2} = \frac{2P}{\pi Eb},$$

$$[A_{ii}]_{11} = u|_{r=a, \theta=0} = -\frac{2P}{\pi E} \ln \frac{a}{d}, \quad [A_{ii}]_{21} = 0, \quad [A_{ii}]_{31} = 0,$$

$$[A_{i(i+1)}]_{11} = v(b, -\pi/2) = -\frac{(1+v)P}{\pi E} - \frac{2P}{\pi E} \ln \frac{b}{d},$$

$$[A_{i(i+1)}]_{21} = -u(b, -\pi/2) = \frac{(1-v)P}{2E},$$

$$[A_{i(i+1)}]_{31} = \frac{1}{2}\left(\frac{\partial v}{\partial r} - \frac{1}{r}\frac{\partial u}{\partial \theta} + \frac{v}{r}\right)_{r=b, \theta=-\pi/2} = -\frac{2P}{\pi Eb}.$$

Next consider the case of a tangential load (see Figure 8). The stress field is given in [Timoshenko and Goodier 1970], and can be integrated to obtain the displacement field:

$$\sigma_r = -\frac{2F}{\pi}\frac{\sin\theta}{r}, \quad \sigma_\theta = 0, \quad \tau_{r\theta} = 0,$$

$$u = -\frac{2F}{\pi E}\sin\theta \ln\frac{r}{d} + \frac{(1-v)F}{\pi E}(\theta\cos\theta - \sin\theta), \tag{9}$$

$$v = -\frac{2F}{\pi E}\cos\theta \ln\frac{r}{d} - \frac{2F}{\pi E}\cos\theta - \frac{(1-v)F}{\pi E}\theta\sin\theta + \frac{2F}{\pi E}\frac{r}{d}, \tag{10}$$

$$\frac{1}{2}\left(\frac{\partial v}{\partial r} - \frac{1}{r}\frac{\partial u}{\partial \theta} + \frac{v}{r}\right) = -\frac{2F}{\pi E}\frac{\cos\theta}{r} + \frac{2F}{\pi E}\frac{1}{d}. \tag{11}$$
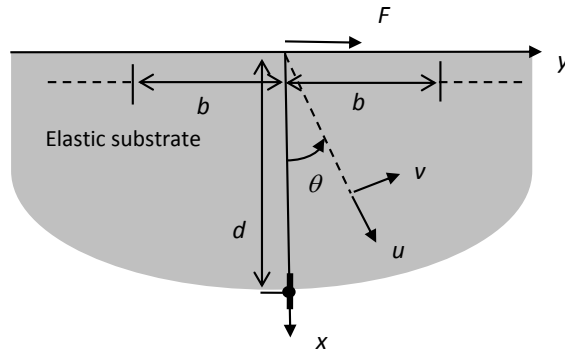
Figure 8. A half-space under a tangential load.

From (9)–(11) we calculate

$$[A_{i(i-1)}]_{12} = -v(b, \pi/2) = -\frac{(1-v)F}{2E} - \frac{2F}{\pi E}\frac{b}{d},$$

$$[A_{i(i-1)}]_{22} = u(b, \pi/2) = -\frac{2F}{\pi E}\ln\frac{b}{d} - \frac{(1-v)F}{\pi E},$$

$$[A_{i(i-1)}]_{32} = \frac{1}{2}\left(\frac{\partial v}{\partial r} - \frac{1}{r}\frac{\partial u}{\partial \theta} + \frac{v}{r}\right)_{r=b,\theta=\pi/2} = \frac{2F}{\pi E}\frac{1}{d},$$

$$[A_{ii}]_{12} = 0, \qquad [A_{ii}]_{22} = v|_{r=a,\theta=0} = -\frac{2F}{\pi E}\ln\frac{a}{d} - \frac{2F}{\pi E} + \frac{2F}{\pi E}\frac{a}{d},$$

$$[A_{ii}]_{32} = \frac{1}{2}\left(\frac{\partial v}{\partial r} - \frac{1}{r}\frac{\partial u}{\partial \theta} + \frac{v}{r}\right)_{r=a,\theta=0} = -\frac{2F}{\pi E}\frac{1}{a} + \frac{2F}{\pi E}\frac{1}{d},$$

$$[A_{i(i+1)}]_{12} = v(b, -\pi/2) = -\frac{(1-v)F}{2E} + \frac{2F}{\pi E}\frac{b}{d},$$

$$[A_{i(i+1)}]_{22} = -u(b, -\pi/2) = -\frac{2F}{\pi E}\ln\frac{b}{d} - \frac{(1-v)F}{\pi E},$$

$$[A_{i(i+1)}]_{32} = \frac{1}{2}\left(\frac{\partial v}{\partial r} - \frac{1}{r}\frac{\partial u}{\partial \theta} + \frac{v}{r}\right)_{r=b,\theta=-\pi/2} = \frac{2F}{\pi E}\frac{1}{d}$$

The last case is shown in Figure 9. The stress field is given in [Timoshenko and Goodier 1970], and can be integrated to obtain the displacement field:

$$\sigma_r = \frac{2M}{\pi}\frac{\sin 2\theta}{r^2}, \quad \sigma_\theta = 0, \quad \tau_{r\theta} = -\frac{M}{\pi}\frac{1+\cos 2\theta}{r^2},$$

$$u = -\frac{2M}{\pi E}\frac{\sin 2\theta}{r} - \frac{4vM}{\pi Ed}\sin\theta, \tag{12}$$

$$v = -\frac{(1-v)M}{\pi E}\frac{\cos 2\theta}{r} - \frac{4vM}{\pi Ed}\cos\theta + \frac{2vM}{\pi Ed^2}r + \frac{(1+v)M}{\pi E}\frac{1}{r}, \tag{13}$$

$$\frac{1}{2}\left(\frac{\partial v}{\partial r} - \frac{1}{r}\frac{\partial u}{\partial \theta} + \frac{v}{r}\right) = \frac{2M}{\pi E}\frac{\cos 2\theta}{r^2} + \frac{2vM}{\pi Ed^2}. \tag{14}$$
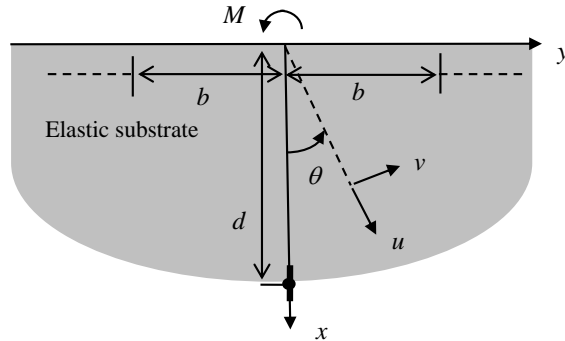
Figure 9. A half-space under a load couple.

From (12)–(14) we calculate

$$[\boldsymbol{A}_{i(i-1)}]_{13} = -\upsilon(b, \pi/2) = -\frac{(1-\upsilon)M}{\pi E}\frac{1}{b} - \frac{2\upsilon M}{\pi Ed^2}b - \frac{(1+\upsilon)M}{\pi E}\frac{1}{b},$$

$$[\boldsymbol{A}_{i(i-1)}]_{23} = u(b, \pi/2) = -\frac{4\upsilon M}{\pi Ed},$$

$$[\boldsymbol{A}_{i(i-1)}]_{33} = \frac{1}{2}\left(\frac{\partial \upsilon}{\partial r} - \frac{1}{r}\frac{\partial u}{\partial \theta} + \frac{\upsilon}{r}\right)_{r=b,\theta=\pi/2} = -\frac{2M}{\pi E}\frac{1}{b^2} + \frac{2\upsilon M}{\pi Ed^2},$$

$$[\boldsymbol{A}_{ii}]_{13} = 0, \quad [\boldsymbol{A}_{ii}]_{23} = \upsilon|_{r=a,\theta=0} = -\frac{(1-\upsilon)M}{\pi E}\frac{1}{a} - \frac{4\upsilon M}{\pi Ed} + \frac{2\upsilon M}{\pi Ed^2}a + \frac{(1+\upsilon)M}{\pi E}\frac{1}{a},$$

$$[\boldsymbol{A}_{ii}]_{33} = \frac{1}{2}\left(\frac{\partial \upsilon}{\partial r} - \frac{1}{r}\frac{\partial u}{\partial \theta} + \frac{\upsilon}{r}\right)_{r=a,\theta=0} = \frac{2M}{\pi E}\frac{1}{a^2} + \frac{2\upsilon M}{\pi Ed^2},$$

$$[\boldsymbol{A}_{i(i+1)}]_{13} = \upsilon(b, -\pi/2) = \frac{(1-\upsilon)M}{\pi E}\frac{1}{b} + \frac{2\upsilon M}{\pi Ed^2}b + \frac{(1+\upsilon)M}{\pi E}\frac{1}{b},$$

$$[\boldsymbol{A}_{i(i+1)}]_{23} = -u(b, -\pi/2) = -\frac{4\upsilon M}{\pi Ed},$$

$$[\boldsymbol{A}_{i(i+1)}]_{33} = \frac{1}{2}\left(\frac{\partial \upsilon}{\partial r} - \frac{1}{r}\frac{\partial u}{\partial \theta} + \frac{\upsilon}{r}\right)_{r=b,\theta=-\pi/2} = -\frac{2M}{\pi E}\frac{1}{b^2} + \frac{2\upsilon M}{\pi Ed^2}$$

For plane-strain problems the following change in material constants is needed:

$$E \to \frac{E}{1-\upsilon^2}, \qquad \upsilon \to \frac{\upsilon}{1-\upsilon}.$$

These fields and interaction coefficients are for beams on a semi-infinite half space. In reality the soft beams are built on a plate with a finite thickness. To compensate for the effect of the finite plate thickness, when comparing with experimental results, we varied d in the above equations and finally chose $d = 1000a$ in our calculations for best agreement with experimental results.

References

[Alfutov 2000] N. A. Alfutov, *Stability of elastic structures*, Springer, Germany, 2000.

[Chen et al. 2008] Z. G. Chen, J. S. Yang, and L. Tan, "Collective buckling of a two-dimensional array of nanoscale columns", *J. Phys. Chem. B.* **112** (2008), 14766–14771.

[Chou et al. 1995] S. Y. Chou, P. R. Krauss, and P. J. Renstrom, "Imprint of sub-25 nm vias and trenches in polymers", *Appl. Phys. Lett.* **67** (1995), 3114–3116.

[Chou et al. 1996] S. Y. Chou, P. R. Krauss, and P. J. Renstrom, "Nanoimprint lithography", *J. Vac. Sci. Technol. B.* **14** (1996), 4129–4133.

[Chuang et al. 2005] W. C. Chuang, C. T. Ho, and W. C. Wang, "Fabrication of a high-resolution periodical structure using a replication process", *Opt. Express.* **13** (2005), 6685–6692.

[Delamarche et al. 1997] E. Delamarche, H. Schmid, B. Michel, and H. Biebuyck, "Stability of molded polydimethylsiloxane microstructures", *Adv. Mater.* **9** (1997), 741–746.

[Evans et al. 2007] B. A. Evans, A. R. Shields, R. L. Carroll, S. Washburn, M. R. Falvo, and R. Superfine, "Magnetically actuated nanorod arrays as biomimetic cilia", *Nano Lett.* **7** (2007), 1428–1434.

[Feng and Li 2009] K. Feng and Z. Li, "Buckling analysis of soft nanostructures in nanoimprinting", *Chin. Phys. Lett.* **26** (2009), 126202.

[Greenhill 1881] A. G. Greenhill, "Determination of the greatest height consistent with stability that a vertical pole or mast can be made, and the greatest height to which a tree of given proportions can grow", *Proc. Cambridge Phil. Soc.* **4** (1881), 65–73.

[Hsia et al. 2005] K. J. Hsia, Y. Huang, E. Menard, J. U. Park, W. Zhou, J. Rogers, and J. M. Fulton, "Collapse of stamps for soft lithography due to interfacial adhesion", *Appl. Phys. Lett.* **86** (2005), 154106.

[Hui et al. 2002] C. Y. Hui, A. Jagota, Y. Y. Lin, and E. J. Kramer, "Constraints on microcontact printing imposed by stamp deformation", *Langmuir.* **18** (2002), 1394–1407.

[Li et al. 2010] Z. Li, K. Feng, J. S. Yang, L. Tan, and H. Lin, "Collective buckling of nonuniform nanobeams interacting through an elastic substrate", *Acta Mech.* **209** (2010), 285–293.

[Lin et al. 2007] H. J. Lin, J. Yang, L. Tan, J. Xu, and Z. Li, "Collective buckling of periodic soft nanostructures on surfaces and promotion for nanolithography", *J. Phys. Chem. C.* **111** (2007), 13348–13356.

[Lin et al. 2010] H. J. Lin, H. L. Du, J. S. Yang, and L. Tan, "Collective buckling of an elastic beam array on an elastic substrate for applications in soft lithography", *Acta Mech.* (2010).

[Liu et al. 2010] Y. M. Liu, D. N. Weiss, and J. Y. Li, "Rapid nanoimprinting and excellent piezoresponse of polymetric ferroelectric nanostructures", *ACS Nano* **4** (2010), 83–90.

[Schmid and Michel 2000] H. Schmid and B. Michel, "Siloxane polymers for high-resolution and high accuracy soft lithography", *Macromolecules.* **33** (2000), 3042–3049.

[Sharp et al. 2004] K. G. Sharp, G. S. Blackman, N. J. Glassmaker, A. Jagota, and C. Y. Hui, "Effect of stamp deformation on the quality of microcontact printing: Theory and experiment", *Langmuir.* **20** (2004), 6430–6438.

[Timoshenko 1936] S. P. Timoshenko, *Theory of elastic stability*, McGraw-Hill, New York, 1936.

[Timoshenko and Goodier 1970] S. P. Timoshenko and J. N. Goodier, *Theory of elasticity*, McGraw-Hill, New Jersy, 1970.

[Xia and Whitesides 1998] Y. N. Xia and G. M. Whitesides, "Soft lithography", *Annu. Rev. Mater. Sci.* **28** (1998), 153–184.

HAOJING LIN: linhaojing1983@gmail.com
Department of Engineering Mechanics, University of Nebraska-Lincoln, P.O. Box 880526, Lincoln, NE 68588-0526, United States

ZIGUANG CHEN: chenziguang@huskers.unl.edu
Department of Engineering Mechanics, University of Nebraska-Lincoln, P.O. Box 880526, Lincoln, NE 68588-0526, United States

JIASHI YANG: jyang1@unl.edu
Department of Engineering Mechanics, University of Nebraska-Lincoln, P.O. Box 880526, Lincoln, NE 68588-0526, United States

LI TAN: ltan4@unl.edu
Department of Engineering Mechanics, University of Nebraska-Lincoln, P.O. Box 880526, Lincoln, NE 68588-0526, United States

JOURNAL OF MECHANICS OF MATERIALS AND STRUCTURES

http://www.jomms.org

Founded by Charles R. Steele and Marie-Louise Steele

Cover design: Alex Scorpan

See inside back cover or http://www.jomms.org for submission guidelines.

Journal of Mechanics of Materials and Structures

Volume 5, No. 3   March 2010